Structural Optimization of trusses considering different buckling models

Marcela A. Juliani[1], Wellison J. S. Gomes[1]

[1]*Center for Optimization and Reliability in Engineering (CORE), Department of Civil Engineering, Federal University of Santa Catarina*
João Pio Duarte da Silva S., 88040-900, Santa Catarina, Brazil
marcelajulianii@gmail.com, wellison.gomes@ufsc.br

Abstract. Constraints related to buckling usually have a significant impact in the structural optimization of trusses, and may be evaluated by employing different models. In this paper, an approach that considers a single global stability constraint, related to the so-called inelastic critical load, is presented and compared with other approaches widely used in the literature. In this approach, each element of the truss is discretized into several frame elements. After applying geometrical initial imperfections in the structure, inelastic buckling can be taken into account implicitly via second-order inelastic analyses. The optimal structures obtained by employing inelastic critical loads for the entire structure, as well as those obtained by considering, for each one of the truss elements, Euler buckling loads or the inelastic buckling loads given in the AISC code, are compared. The optimization problems addressed herein may demand high computational efforts, especially for the inelastic analyses, thus a previously proposed optimization framework based on surrogate models is employed. As a result, higher objective function values occur when the model from the AISC code is used. Furthermore, the inelastic model can lead to structures with large displacements, so the displacements must be limited to result in more realistic designs.

Keywords: Buckling, Nonlinearities, Structural optimization, Surrogate models

1 Introduction

Truss structures are widely employed in civil construction, such as in bridges, roofs and transmission towers. Thus, several authors have been researching the field of truss optimization, in order to find safe structures with the lowest cost. In this type of problem, one of the most used constraints is the one related to the buckling of the bars. According to Yoo and Lee [1], this phenomenon corresponds to the lateral deflection of structural elements, usually straight and slender, in relation to their initial longitudinal positions, due to compression. In general, buckling occurs abruptly and can lead to partial or total failure of the structure.

Lateral buckling of bars can be evaluated by different models. Most of the time, this phenomenon is taken into account by confronting the stress in each structural element, obtained through first-order elastic analysis, with a critical buckling stress, which depends on the material and geometric properties of the analyzed element. Many authors who adopt this approach use Euler's formulation to determine the referred allowable stress, which considers that the material has linear-elastic behavior, representing the so-called elastic buckling [2, 3]. On the other hand, there are also empirical expressions that seek to consider the response that the material may present beyond the limits of the idealized linear-elastic regime, such as the formulations provided by the AISC-360 [4] code, representing the so-called inelastic buckling [5, 6].

Although the scenarios presented above are the most used in the literature, due to their simplicity and low computational cost, other models can lead to a better representation of the structural behavior. Modeling the buckling of each element individually, can result in a limited analysis for optimization problems of large structures, since it does not take into account the behavior of the structure as a whole. In this sense, some researchers consider the buckling through a single global stability constraint for the entire structure, represented by a critical load. In this approach, each truss element is discretized into several frame elements, in some cases with moment releases at hinged connections. From this model, the elastic critical load can be determined through an eigenvalue analysis, as in Torii et al. [7] and Mitjana et al. [8], or also through second-order elastic analyses with geometrical initial

imperfections in the structure, as in Madah and Amir [9] and Varma et al. [10].

As shown, there are several studies on optimization that use different models to represent buckling. However, the differences in the optimal configurations obtained by these models are hardly discussed. Furthermore, despite the advances in the representation of the structural behavior, there is a lack of optimization studies that consider the effect of the inelastic behavior of the material in the critical load. In this context, this paper presents an analysis of the optimal configuration of trusses, considering three distinct constraint scenarios: scenario 1 considers elastic buckling constraint, characterized by the application of Euler's critical stress; scenario 2 uses the formulation given in the AISC-360 [4] code to determine the critical stress; and scenario 3 considers inelastic buckling constraint, represented by a single stability criterion. This study is an extension of a previously published paper [11], so herein a new scenario and a larger structure are evaluated, and an optimization method based on metamodels is used to deal with the high computational effort demanded in the solutions of the problems.

The remainder of this paper is organized as follows: section 2 presents the methodology applied in this research, such as the formulation of the buckling models, as well as the optimization method; section 3 presents the application of the proposed approach to two numerical examples; conclusions and discussions about the results obtained in this paper are presented in section 4.

2 Optimization and buckling models

The optimization problem addressed herein consists of finding the values of the design variables **x** that minimize the objective function $f(\mathbf{x})$, subject to inequality constraints $g_i(\mathbf{x}) \leq 0$ and to lower and upper bounds of each variable x_j, with $i = 1, ..., n$ and $j = 1, ..., m$, where n and m are the numbers of constraints and design variables, respectively. In this section, the three constraint scenarios evaluated are presented, as well as a brief description of the optimization method. All codes are developed in MATLAB [12] and the software MASTAN2 [13] is used for structural analysis.

2.1 Euler's critical stress: scenario 1

In this scenario, a first-order elastic analysis of the truss is performed, and then for each one of the n_{bar} bars, the following checks are made: if the i-th structural element is under compression, the absolute value of its stress $|\sigma_i(\mathbf{x})|$ must not exceed the lowest stress between the yield stress σ_{y_i} and the Euler buckling stress $\sigma_{e_i}(\mathbf{x})$; if the i-th structural element is under tension, its stress $\sigma_i(\mathbf{x})$ must not exceed σ_{y_i}. Equation (1) summarize this procedure, where E is the modulus of elasticity of the material, I and A are, respectively, the moment of inertia and the cross-sectional area of the structural element and L_e is the buckling length, taken equal to the length of the bar in the case of trusses.

$$g_i(\mathbf{x}) \underset{(i=1,\ldots,n_{bar})}{=} \begin{cases} \dfrac{\sigma_i(\mathbf{x})}{\sigma_{y_i}} - 1 \leq 0, \ \text{ if } \ \sigma_i(\mathbf{x}) > 0; \\ \dfrac{|\sigma_i(\mathbf{x})|}{\min(\sigma_{y_i}, \sigma_{e_i}(\mathbf{x}))} - 1 \leq 0, \ \text{ if } \ \sigma_i(\mathbf{x}) < 0, \ \text{ with } \ \sigma_{e_i}(\mathbf{x}) = \dfrac{\pi^2 E_i I_i}{A_i L_{e_i}^2}. \end{cases} \tag{1}$$

2.2 Allowable stress according to AISC: scenario 2

According to AISC-360 [4], there are two equations that govern the strength of bars under compression, which are based on the limit state of flexural buckling [14]: the first represents elastic buckling, which consists of a portion of the Euler critical stress; the second is an empirical relationship for the inelastic range of buckling. Both equations include the effects of residual stresses and initial out-of-straightness. Thus, the critical stress for compressed bars is given by eq. (2), where r is the radius of gyration. Similar to scenario 1, the stress in the elements under tension is limited to σ_y and the stress in the elements under compression cannot exceed σ_{cr}.

$$\begin{array}{ll} \text{(a) If } \ \dfrac{L_e}{r} > 4.71\sqrt{\dfrac{E}{\sigma_y}} \rightarrow \text{Elastic buckling:} & \text{(b) If } \ \dfrac{L_e}{r} \leq 4.71\sqrt{\dfrac{E}{\sigma_y}} \rightarrow \text{Inelastic buckling:} \\ \sigma_{cr} = 0.877\sigma_e & \sigma_{cr} = \left(0.658^{\frac{\sigma_y}{\sigma_e}}\right)\sigma_y \end{array} \tag{2}$$

2.3 Inelastic critical load: scenario 3

In this scenario, a single constraint is considered, given by

$$g(\mathbf{x}) = \frac{P}{P_{cr}(\mathbf{x})} - 1 \leq 0, \tag{3}$$

where P is the applied load and $P_{cr}(\mathbf{x})$ is the critical load, which is the maximum load value that the structure can handle before reaching failure. In order to incorporate the possibility of buckling and yielding in the computation of the critical load, it is necessary to impose initial imperfections to each bar of the structure and to perform inelastic and geometrically nonlinear structural analyses. To do so, in this paper the initial imperfections are based on some of the first buckling modes of the structure and the materials are assumed to have elastic-plastic characteristics, according to the formulations of McGuire et al. [13].

Therefore, in this scenario, the following procedure is carried out: first, an eigenvalue analysis of the structure is performed; then, for each buckling mode considered, the critical load is calculated by second-order inelastic analysis, taking into account a perturbation in the nodal coordinates of the structure according to $\mathbf{c} = \mathbf{c}_0 + \alpha\mathbf{u}$, where the vectors $\mathbf{c}_0$ and $\mathbf{c}$ are the nodal coordinates before and after the perturbation, respectively, $\mathbf{u}$ is the vector of nodal displacements, according the buckling mode considered in the eigenvalue analysis, and α is a reduction factor; finally, eq. (3) is checked for each one of the critical loads evaluated. In structural analysis, truss bars are modeled using several frame elements with moment releases at hinged connections. So, elements that are connected to hinges are modeled as fixed-hinge frame element while others are modeled as fixed-fixed elements.

The pinned end column shown in Fig. 1(a), previously studied by McGuire et al. [13], is analyzed herein to define the value of α and to validate the three buckling models. The parameters of the column are: A = 9.13 in^2 (58.9031 cm^2), I = 37.1 in^4 (1544.2186 cm^4), plastic section modulus Z = 14.1 in^3 (231.0576 cm^3), L = 120 in (304.8 cm), E = 29000 ksi (200 GPa) and σ_y = 50 ksi (345 MPa).

First, to define the reduction factor, the critical loads are obtained for increasing values of α and compared with the theoretical load provided by McGuire et al. [13], as shown in Fig. 1(b). It is observed that, although all curves converge to the theoretical load, the displacements obtained are different from each other. Varma et al. [10] notes that with the increase in the magnitude of the imperfection, the load-displacement curve for elastic analysis shifts away from the ideal situation (sudden large displacement), which is also observed herein for inelastic analysis. However, when no imperfection is applied (α = 0) the model cannot capture the buckling configuration, resulting in null lateral displacements. Thus, α = 0.10% is adopted in this paper, since it is able to identify the instability without major influence on the structural displacements.

To verify the three scenarios, the resistance curves of the column are obtained for several values of slenderness ratio. Figure 1(c) shows the curves, which are very similar to those provided by McGuire et al. [13]. Note that the biggest differences between the models occur for slenderness ratio between 25 and 125. For slenderness smaller than 25, the resistance is basically given by the yield stress, and for slenderness greater than 125, the buckling is characterized as elastic. Furthermore, the behavior of scenario 3 is similar to that of scenario 2, with the biggest difference between them being 15%. Scenario 1 provides resistances up to 33% and 52% greater than scenario 3 and 2, respectively.

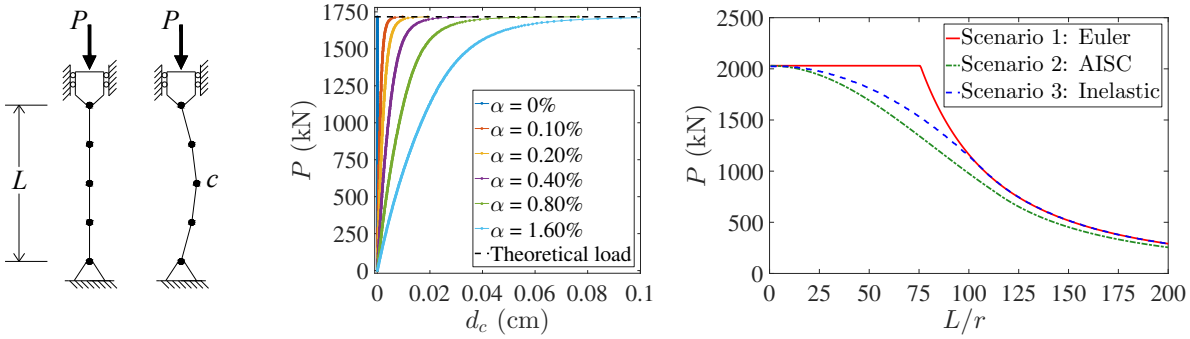

(a) Model of the column and its perturbation

(b) Convergence of the inelastic critical load

(c) Resistance curves

Figure 1. Pinned end column problem

2.4 Optimization framework

Surrogate model is a mathematical model constructed based on a limited data set from a computational or physical experiment. Thus, it is possible to use the surrogate model in order to predict the results assumed by the experiment, without performing it [15]. In the context of optimization, surrogate models can be used to replace objective and/or constraint functions, when these functions demand high computational efforts to be evaluated.

The optimization framework used herein is similar to the one presented in Juliani and Gomes [16], which uses the Kriging metamodel and performs three search strategies to improve the accuracy of the surrogate model and to look for the optimum during the optimization process: local search, global search and refinement. The main modification performed herein is that only the constraints are replaced by the metamodel, since these are the functions that may demand high computational effort in the evaluated scenarios, especially for the inelastic analysis. Furthermore, the refinement step adopted corresponds to the solution of the surrogate optimization problem via a gradient-based method. The optimum found in this step is inserted into the data set to improve Kriging accuracy.

This method showed promise for several examples, with different types of structures, design variables, objective functions and constraints, keeping the accuracy of the solution and reducing the number of constraints evaluations and computational time.

3 Numerical examples

This section presents two numerical examples. The first, a pinned end column, is an introductory example, to visualize the behavior of the different scenarios. The second corresponds to a model based on a British bridge. In both examples, each scenario is run 10 times, considering different initial points for the optimization framework, related to different seeds of the pseudo-random number generator. The best result obtained is taken as the final result of the optimization process. In the structural analysis of scenario 3, the maximum applied load ratio is 1.1 and 110 load increments are used. Furthermore, the first three modes of buckling are considered as imperfection.

3.1 Pinned end column

The column studied here is the one presented in section 2.3. The objective function corresponds to the cross-sectional area, which is adopted as tubular. The design variables are the mean diameter d and the thickness t of the cross section. The lower and upper bounds are 2 in (5.08 cm) $\leq d \leq$ 10 in (25.4 cm) and 0.2 in (0.508 cm) $\leq t \leq$ 0.6 in (1.524 cm), and P = 100 kips (444.8 kN).

Table 1 shows the optimization results, where FE refers to the number of constraint evaluations. The slenderness ratio of scenarios 1 to 3 are, respectively, 85, 73 and 78, which correspond to the region where the buckling models are distinct from each other in Fig 1(c). In this situation, eq. (2) indicates that the optimum of its scenario is in the inelastic region. As expected, it is observed that the optimal structure for the Euler constraint is the cheapest, and that the based in the AISC-360 [4] code is the most expensive. Also, the optimal designs with higher values satisfy the constraint scenarios that presented optimal designs with lower values, whereas the opposite is not valid. Figure 2 shows the surface of the constraints along the search space. It can be observed that scenario 3 presents some discontinuities, related to the load increments of the structural analysis. The more increments, the less discontinuities appear on the surface; however, the computational effort also increases. This fact can be a challenge, making it difficult to solve optimization problems involving many design variables and large structures. This may also impair the accuracy of the metamodels.

Table 1. Optimization results: Pinned end column

	d (cm)	t (cm)	A (cm^2)	max($\mathbf{g}$)	Mean	Std.	FE	Time (min)
Scenario 1: Euler	10.1546	0.5080	16.2061	-2$\times10^{-6}$	16.3445	0.4369	39	0.98
Scenario 2: AISC	11.8767	0.5080	18.9543	-2$\times10^{-6}$	18.9745	0.0430	39	0.77
Scenario 3: Inelastic	10.9932	0.5080	17.5443	0	17.7072	0.3366	57	1.60

3.2 A model of Forth bridge

Previously analyzed by Kaveh and Khayatazad [5], this problem is based on a British bridge, as shown in Fig. 3. In the present paper, the bars are categorized into 3 groups and the structure is symmetrical in relation to

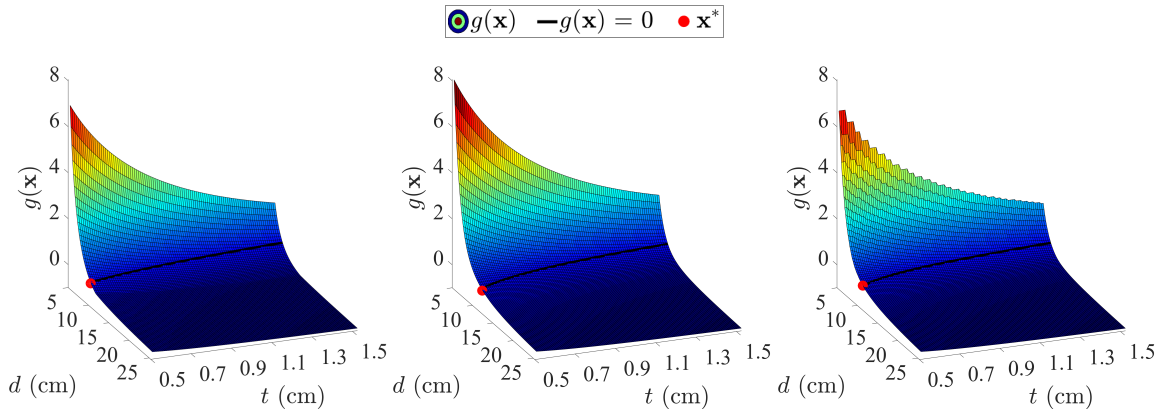

(a) Scenario 1: Euler (b) Scenario 2: AISC (c) Scenario 3: Inelastic

Figure 2. Constraint scenarios for different buckling models: Pinned end column

the middle vertical plane. The search space for the cross section areas are 25 cm^2 $\leq A \leq$ 100 cm^2 and the vertical position of nodes 2 to 11 can vary $\pm$1.4 m. The objective function corresponds to the mass of the structure and the self-weight is considered in the load. The material has E = 210 GPa, σ_y = 250 MPa and specific weight of 7.8 ton/m^3. The relationship $I = 0.4872A^{2.1858}$ and $Z = 0.6277A^{1.5931}$ is used, based on the hollow circular sections available in AISC [17].

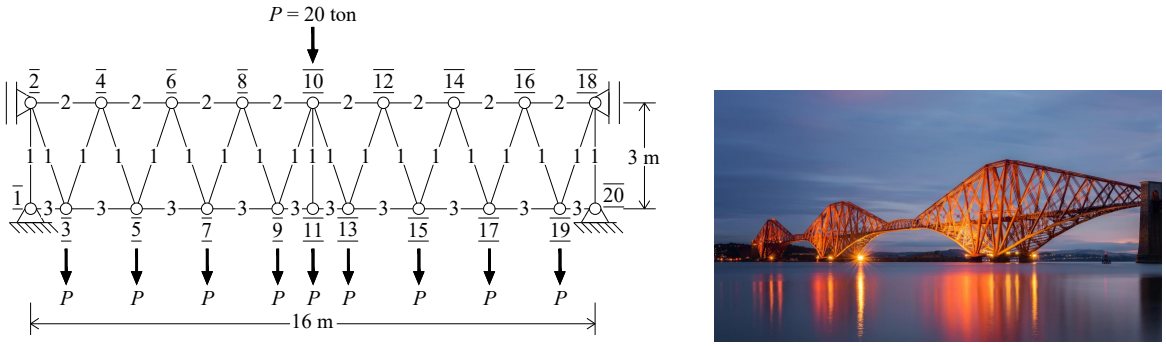

(a) Model (b) Forth bridge [18]

Figure 3. Forth bridge problem

The optimization results, presented in Table 2, show that the inelastic scenario led to the lightest structure, while the scenario based in the code resulted in the heavier structure. It can be seen in the load-displacement curve of Fig. 4 that scenario 3 presented vertical displacement in mid span approximately 100 times greater than the other scenarios, making this result inconsistent with a viable structural design. It is noteworthy that the optimal designs for the first two scenarios, when applied in the inelastic model, do not lead to large displacements. The plastification of bars allows a better redistribution of efforts, so that when this phenomenon occurs and does not lead to the collapse of the structure as a whole, the structural model is able to support more load. In the optimal structure of scenario 3, several bars reached the yield stress without an instability that could lead to the collapse of the structure; however, this plastification led to large displacements. Among the optimal responses obtained in the runs of scenario 3, the one with the smallest displacement can be presented as a more realistic solution. This configuration has 1763.2920 kg and displacement of -3.47 cm in the mid span. The configurations and the normal stresses of these solutions are illustrated in Fig. 5. All solutions resulted in a shape similar to the original bridge, except for the inelastic result with large displacement. In addition, the optimal structure of scenario 2 meets the constraints of all scenarios; however, the other structures only meet the constraints of their own scenarios.

4 Conclusions

This paper presented a comparison between three distinct buckling constraints scenarios: scenario 1 considers elastic buckling; scenario 2 uses the formulation given in the AISC-360 [4]; and scenario 3 considers inelastic

Table 2. Optimization results: Forth bridge

Design	Scenario 1: Euler	Scenario 2: AISC	Scenario 3: Inelastic	Design	Scenario 1: Euler	Scenario 2: AISC	Scenario 3: Inelastic
y_2,y_{18} (m)	0.6337	1.0831	-1.0765	A_1 (cm^2)	25.0000	25.0000	25.0000
y_3,y_{19} (m)	0.5422	1.0586	1.4000	A_2 (cm^2)	33.3942	33.8713	25.0000
y_4,y_{16} (m)	0.2235	0.4569	-1.4000	A_3 (cm^2)	32.3990	32.4175	27.7639
y_5,y_{17} (m)	1.4000	1.4000	0.4400	Mass (kg)	1740.5315	1825.4670	1478.4984
y_6,y_{14} (m)	-1.4000	-1.4000	-1.4000	max($\mathbf{g}$)	-0.0008	-0.0012	-0.0001
y_7,y_{15} (m)	0.2185	-0.0443	0.1061	Mean	1838.3535	1902.8457	1756.6890
y_8,y_{12} (m)	-1.4000	-1.4000	-1.4000	Std.	57.2237	85.6005	108.6218
y_9,y_{13} (m)	-0.3881	-0.6104	-0.0894	FE	750	757	754
y_{10} (m)	-1.4000	-1.4000	0.8329	Time (min)	19.18	20.66	77.86
y_{11} (m)	-0.5650	-0.8543	-0.4094				

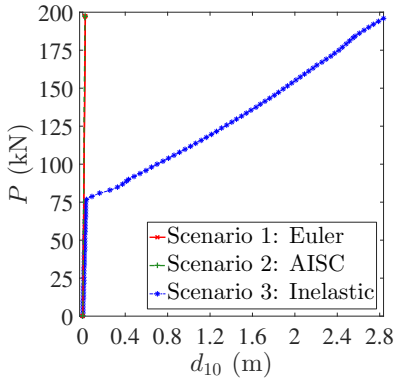

Figure 4. Load-displacement curve: Forth bridge

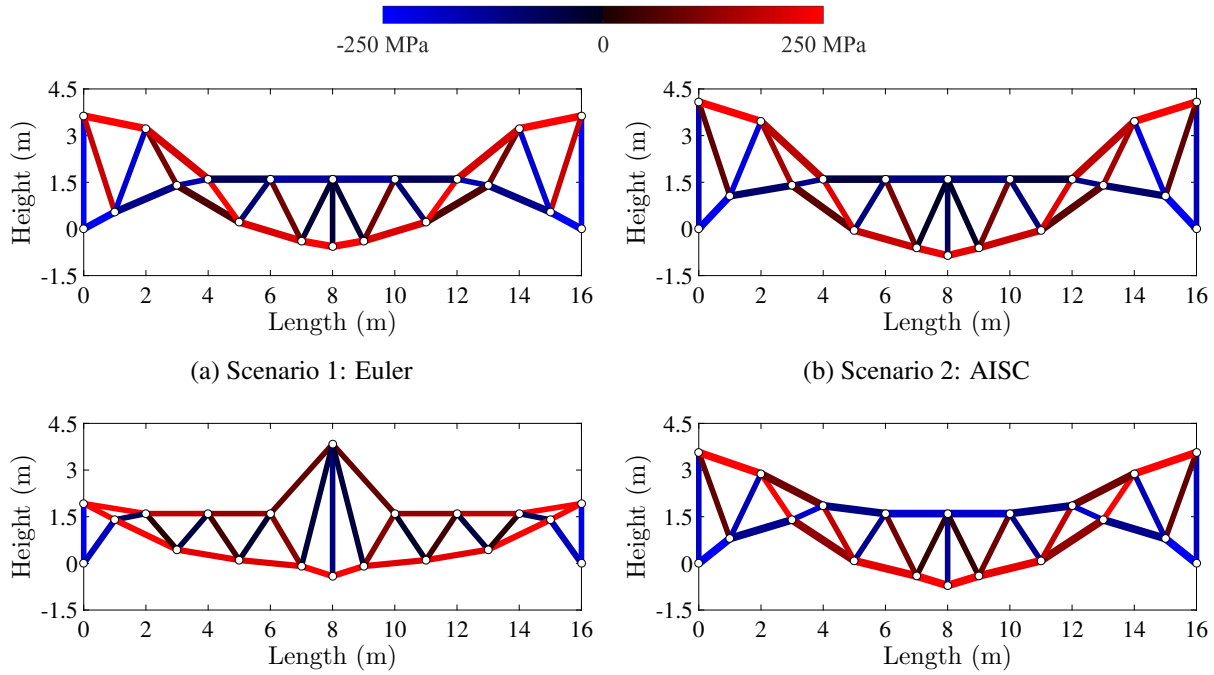

(a) Scenario 1: Euler

(b) Scenario 2: AISC

(c) Scenario 3: Inelastic

(d) Inelastic with low displacement

Figure 5. Optimal configurations and normal stress distribution: Forth bridge

buckling. It was observed that the scenario based in the code presents a resistance curve, for a single column, similar to that of the inelastic scenario. However, it is noteworthy that the inelastic model takes into account the global behavior of the structure. Thus, if a structure with more elements is analyzed, the scenarios can lead to quite different results. Two optimization problems were evaluated. In both examples, the optimal configuration of scenario 2 provided higher values of objective function and also met the constraints of the other scenarios. Furthermore, it was found that the inelastic buckling model can result in a lighter structure, but with large displacements. This can occur due to the plastification of the bars without the occurrence of a generalized instability. Thus, the importance of considering maximum allowable displacements when using inelastic models is highlighted.

Acknowledgements. The authors gratefully acknowledge the financial support from Scientific and Technological Research Support Foundation of Santa Catarina State and Coordination of Superior Level Staff Improvement (FAPESC/CAPES, public call nº 03/2017) and National Council for Scientific and Technological Development (CNPq, via grant 302489/2017-7).

Authorship statement. The authors hereby confirm that they are the sole liable persons responsible for the authorship of this work, and that all material that has been herein included as part of the present paper is either the property (and authorship) of the authors, or has the permission of the owners to be included here.

References

[1] C. H. Yoo and S. C. Lee. *Stability of Structures: Principles and Applications*. Elsevier Inc, Burlington, MA, USA, 2011.
[2] S. Gholizadeh. Layout optimization of truss structures by hybridizing cellular automata and particle swarm optimization. *Computers & Structures*, vol. 125, pp. 86–99, 2013.
[3] E. Ficarella, L. Lamberti, and S. O. Degertekin. Comparison of three novel hybrid metaheuristic algorithms for structural optimization problems. *Computers & Structures*, vol. 244, 2021.
[4] AISC-360. *Specification for Structural Steel Buildings: ANSI/AISC 360-16*. American Institute of Steel Construction, 2016.
[5] A. Kaveh and M. Khayatazad. Ray optimization for size and shape optimization of truss structures. *Computers & Structures*, vol. 117, pp. 82–94, 2013.
[6] A. C. C. Lemonge, J. P. G. Carvalho, P. H. Hallak, and D. E. C. Vargas. Multi-objective truss structural optimization considering natural frequencies of vibration and global stability. *Expert Systems with Applications*, vol. 165, 2021.
[7] A. J. Torii, R. H. Lopez, and L. F. F. Miguel. Modeling of global and local stability in optimization of truss-like structures using frame elements. *Structural and Multidisciplinary Optimization*, vol. 51, n. 6, pp. 1187–1198, 2015.
[8] F. Mitjana, S. Cafieri, F. Bugarin, C. Gogu, and F. Castanie. Optimization of structures under buckling constraints using frame elements. *Engineering Optimization*, vol. 51, n. 1, pp. 140–159, 2018.
[9] H. Madah and O. Amir. Truss optimization with buckling considerations using geometrically nonlinear beam modeling. *Computers & Structures*, vol. 192, pp. 233–247, 2017.
[10] T. V. Varma, S. Sarkar, and G. Mondal. Buckling restrained sizing and shape optimization of truss structures. *Journal of Structural Engineering*, vol. 145, n. 5, 2020.
[11] M. A. Juliani, M. O. Milanez, and W. J. S. Gomes. Structural optimization of trusses under elastic and inelastic buckling constraints. *XL Ibero-Latin American Congress on Computational Methods in Engineering (CILAMCE)*, 2019.
[12] MathWorks. *MATLAB: Primer*. Natick, MA, EUA, 2017.
[13] W. McGuire, R. H. Gallagher, and R. D. Ziemian. *Matrix Structural Analysis*. 2nd edition, 2014.
[14] AISC-LRFD. *Manual of steel construction: Load & Resistance Factor Design*. American Institute of Steel Construction, 1994.
[15] A. I. J. Forrester, A. Sóbester, and A. J. Keane. *Engineering Design via Surrogate Modelling: A Practical Guide*. John Wiley and Sons, Chichester, 2008.
[16] M. A. Juliani and W. J. S. Gomes. Comparison of kriging and radial basis function surrogate models applied to a global optimization framework. *XLI Ibero-Latin American Congress on Computational Methods in Engineering (CILAMCE)*, 2020.
[17] AISC. *Shapes Database v15.0*. American Institute of Steel Construction, 2017.
[18] The times. *Privacy fears over Forth Bridge plans*. https://www.thetimes.co.uk/article/privacy-fears-over-forth-bridge-plans-xpbzq36p2, UK, 2020.